HHS Public Access

Author manuscript

Ophthalmol Retina. Author manuscript; available in PMC 2021 February 01.

Published in final edited form as:

Ophthalmol Retina. 2020 February ; 4(2): 204–215. doi:10.1016/j.oret.2019.09.012.

Age-related changes in choroidal thickness and the volume of vessels and stroma using swept source OCT and fully automated algorithms

Hao Zhou, PhD[1], **Yining Dai, MD**[1], **Cancan Lyu, MD**[2], **Jila Noorikolouri, MD**[2], **William J. Feuer, MS**[2], **Zhongdi Chu, PhD**[1], **Qinqin Zhang, PhD**[1], **Luis de Sisternes, PhD**[3], **Mary K. Durbin, PhD**[3], **Giovanni Gregori, PhD**[2], **Philip J. Rosenfeld, MD**[2], **Ruikang K. Wang, PhD**[1,4,*]

[1]Department of Bioengineering, University of Washington, Seattle, WA 98105, USA

[2]Department of Ophthalmology, Bascom Palmer Eye Institute, University of Miami Miller School of Medicine, Miami, FL 33136, USA

[3]Research and Development, Carl Zeiss Meditec, Inc. Dublin, CA 94568, USA

[4]Department of Ophthalmology, University of Washington, Seattle, WA 98105, USA

Abstract

Purpose: To determine age-related changes in choroidal thickness and the volume of choroidal vessels and stroma using automated algorithms based on structural swept source OCT (SS-OCT) scans.

Design: Prospective and observational study.

Participants: One hundred and forty-four normal subjects with ages ranged from 20 to 88 years.

Methods: A previously reported strategy was used to automatically segment the choroid using SS-OCT structural images. Attenuation correction was applied on B-scans to enhance the choroidal contrast and facilitate more accurate automatic segmentation of the 3D choroidal vessel and stroma. The parameters investigated included mean choroid thickness (MCT), choroidal vessel volume (CVV), choroidal stroma volume (CSV), choroid vascularity index (CVI), and the choroidal stroma-to-vessel volume ratio (CSVR). Correlations between MCT and choroidal vessel metrics of CVV, CSV, CVI, and CSVR were studied. Regional distributions of MCT and CVI were analyzed using a grid centered on the fovea. Age-related changes in MCT, CVV, CSV, and CVI were studied in the whole scanning region, as well as in the sub-regions of the grids.

Main Outcome Measures: Age-related changes in MCT, CVV, CSV, and CVI using 6×6 mm and 12×12 mm SS-OCT scans.

Results: The automated choroid segmentations were validated against manual segmentations, and MCT measurements were shown to be in good agreement ($P<0.0001$). CVV and CSV showed significant correlations with MCT (all $P < 0.0001$). Interestingly, CVI and CSVR were constant with little variation among all subjects regardless of age and MCT (61.1±1.8% and 0.64±0.05, respectively). Measurements on 12×12 and 6×6 mm scans showed excellent agreement in all scan

* wangrk@uw.edu.

regions (all P < 0.0001). While choroid thickness (CT) and choroid volume (CV), which includes both choroidal vessels and stroma, decreases with age (all P < 0.0001), the CVI and CSVR vary little among all ages in all regions.

Conclusions: While MCT, CVV, and CSV decrease with age, the CVI and CSVR remain constant in all regions with age. Ongoing studies are using these automated algorithms on SS-OCT structural datasets to investigate the diagnostic usefulness of these choroidal parameters in a myriad of ocular and systemic diseases.

INTRODUCTION

The choroid, located between the retina and sclera, is a layer comprised of blood vessels and stroma and is mainly responsible for delivering nutrients and supporting the metabolic exchange between the circulation and the retinal pigment epithelium (RPE) and photoreceptors.[1,2] Other important roles include ocular thermoregulation and providing a blood supply for the proximal optic nerve.[3,4] Clinical imaging technologies such as color fundus photography, fundus autofluorescence (FAF), fluorescein angiography (FA), indocyanine green angiography (ICGA) provide some direct and indirect information about the health of the choroid, but these methods cannot provide depth-resolved quantitative information about the choroid.[5,6] Optical coherence tomography (OCT) has provided some cross-sectional quantitative information about choroidal thickness and choroidal vessel dimensions, but most of the reports are limited to B-scans using spectral domain OCT (SD-OCT) and a strategy known as enhanced depth imaging.[7–9] Swept source OCT (SS-OCT) uses a longer wavelength of light at about 1060 nm compared with SD-OCT at 840 nm, and this longer wavelength allows for better imaging of the choroid due to better penetration through the RPE, less sensitivity roll-off, and the use of a higher laser energy, which results in better signal-to-noise image quality.[10–12]

Most of the previous reports on choroidal thickness and choroidal vessel measurements have been limited to SD-OCT B-scans and involved manual or semi-automated methods.[9,13–16] For SS-OCT scans, manual techniques for B-scans have been reported to date[17,18] and measurements of choroidal thickness and vessel volumes have not been reported from widefield three-dimensional (3D) SS-OCT datasets. Using SS-OCT foveal B-scans, Cheng et al. measured choroidal vessel densities from SS-OCT foveal B-scans[9] and reported on choroidal vascularity index (CVI) as a measure of choroidal vascular status from B-scans. In their report, a 1.5 mm segmentation block in the subfoveal choroidal area was binarized to segment luminal area and the CVI was calculated as luminal area divided by total area of the selected block. CVI was demonstrated to be less variable than sub-foveal choroid thickness measurements, and therefore, might be a more useful marker for evaluating choroidal diseases. However, such measurements are limited to a very small region of foveal B-scans. A similar metric was measured from widefield OCT (WF-OCT) horizontal and vertical B-scans.[13] The horizontal scans were separated into macular, nasal and temporal segments and the vertical scans were separated into macular, superior and inferior segments. The study showed that in young normal subjects the CVI of the macular area was significantly smaller than other regions. In another study, choroidal area, vessel area and stromal area were measured from a single 12 mm B-scan.[14]

A better strategy for visualizing the choroidal vasculature over a wider region involves the use of en face imaging of a volumetric SS-OCT dataset.[19,20] Previously, we used *en face* imaging of a 12×12 mm scan to show that choroidal vessel densities had a clear relationship between mean choroid thickness and the density of large choroidal vessels. In this report, eyes with age-related macular degeneration, either with or without reticular pseudodrusen (RPD), were compared, and eyes with RPD were found to have global thinning of the choroid. This choroidal thinning was associated with a decrease in choroidal vessel densities in different regions within the 12×12 mm field of view (FOV) centered on the fovea.[20] We concluded that choroidal thickness and its vasculature were closely related, and pathological conditions associated with choroidal thickness could have an underlying vascular basis for a wide range of ocular diseases. To further understand this relationship in normal aging and ocular diseases, we set out to explore different metrics for assessing the choroidal vasculature.

Recently, we developed a novel, practical approach to automatically segment the choroidal vasculature and the choroid using 3D SS-OCT datasets.[21] This method only used structural SS-OCT scans and achieved an angiographic-like image of the choroidal vessels, similar to ICG angiography, but without the need for invasive dyes or SS-OCTA. While OCTA has become a clinically impactful vascular imaging technique in ophthalmology, but cannot directly measure flow in the larger choroidal vessels.[22–24] This inability to measure flow from the larger choroidal vessels results from the fact that when light passes through choroid, the majority of the photons scatter forward through blood, and the small amount of light that is reflected ends up being scattered by the RPE so there is no detectable signal, and the large choroidal vessels appear dark on structural OCT images.[25,26] Thus, the dark appearance of the choroidal vessels on the OCT scans can be used as a surrogate to represent the choroidal vessels. However, when measuring the boundaries of the choroid, the 3D segmentation of the choroidal scleral interface can be poorly visualized due to the severe light attenuation within the choroid. To mitigate this issue, we developed a “gain control” method, which is similar to the method that is widely applied in ultrasound imaging.[27] This method first uses attenuation compensation to compensate for the attenuated OCT signal along each A-scan to enhance the contrast of choroidal vessels and stroma, especially at the interface between choroid and sclera. The resulting OCT volume with higher inter-layer contrast in which shadowing effects were eliminated was then used to develop an automated segmentation algorithm for the choroid using multiple graph search methods.[21] With this approach, we were able to automatically segment choroidal vessels in 3D from the whole 12×12 mm choroidal slab.

In this report, we studied normal eyes over a wide range of ages and identified several useful metrics for assessing the 3D choroidal vasculature. These metrics include the mean choroid thickness (MCT), choroid vessel volume (CVV), choroid stroma volume (CSV), choroidal vessel volume density (i.e. choroidal vascularity index (CVI)) and choroidal stroma-to-vessel volume ratio (CSVR). Using this automated method on conventional SS-OCT structural scans, we assessed the spatial and temporal variations in choroidal vasculature over the entire FOV.

Methods

Study subjects with normal eyes were enrolled as part of a prospective OCT study approved by the Institutional Review Board of Medical Sciences Subcommittee at University of Miami, Miller School of Medicine. IRB-approved consents were obtained from all subjects before scanning and the use of unidentified personal and medical information. All procedures adhered to the tenets of Declaration of Helsinki. Subjects were recruited with a normal ocular history, no visual complains, no retinal, optic nerve, or choroidal pathologies, no history of diabetes, and no history of uncontrolled hypertension.[28]

The enrolled subjects were scanned using a SS-OCT instrument (Plex® ELITE, Carl Zeiss Meditec Inc., Dublin, CA) with a central wavelength of 1060 nm, a bandwidth of 100 nm, a scanning rate of 100 kHz with a full-width at half-maximum axial resolution of approximately 5 microns in tissue, a lateral resolution at the retinal surface estimated at approximately 20 micron, and an A-scan depth of 3.0 mm (1536 pixels) in tissue. The 12×12 mm and 6×6 mm macular scans were obtained and centered on the fovea. The scans consisted of 500 A-scans per B-scans and 2 repeated B-scans at each of the 500 B-scan positions. Each scan was reviewed for quality and signal strength. Scans with motion artifacts or with a signal strength less than 7 were excluded from the analyses. Axial length was measured using a noncontact biometry instrument (IOL Master, Carl Zeiss Meditec).

The choroidal slab was automatically segmented via an algorithm that was previously developed and validated.[21] Briefly, the algorithm consists of attenuation compensation and exponentiation that were consecutively applied to the OCT structural scans to enhance the contrast of choroid-sclera interface (Figure 1 A&B), the concept of which is similar to “gain control” in ultrasound imaging.[27] The intensity at each pixel is converted as:

$$D_{Attn-corr}(z) = \frac{D_A^2(z)}{2\sum_{z+1}^{n} D_A^2(z)} \quad (1)$$

where D_A and $D_{Attn\text{-}corr}$ is the signal before and after attenuation correction, z is the depth location, and n is the total number of pixels along A-scan.

The optic discs in the 12×12 mm scans were automatically detected from *en face* sum projection of the whole volume and were excluded. The Bruch’s membrane and the outer border of choroidal vessels were then automatically detected through graph search methods (Figure 1C). With attenuation correction, we have shown that the method increased the accuracy of the CSI segmentation from 74.5 ± 8.0% to 91.8 ± 3.7% ($P < 0.01$).[21] The color-coded *en face* choroidal thickness map was then generated as the distance between the two detected boundaries of the Bruch’s membrane and choroid-scleral interface (Figure 1D).

Manual segmentations of the choroid were performed on a subset of the normal database by two experts [CL and JN] and reviewed by GG to assure consistency. Consensus segmentation was reached on all cases.

Mean choroidal thickness (MCT) was calculated as the mean value of the thickness over the entire scanning region (excluding optic disc):

$$\mathrm{MCT} = \frac{\sum T}{N_{enface}} \quad (2)$$

where T is the value of each pixel in the *en face* choroid thickness map and N_{enface} is the total number of pixels in the map (excluding optic disc). A larger MCT indicates a thicker choroid.

Three-dimensional representation of choroidal vessels was obtained by segmenting the vessels from the choroid slab of the OCT structure scans (Figure 1E, F). This was performed after "gain control" compensation of the OCT signals along their depth (Figure 1A, B) and after the automated segmentation of choroid (Figure 1C&D). A moving average among three adjacent B-scans was applied to enhance the signal-to-noise ratio for each B-scan followed with histogram equalization. A global image threshold using Otsu's method was applied to segment dark regions in the choroid,[9] which was then inverted to represent the choroidal vessels (Figure 1F). In each volume scan, choroid vessel volume (CVV) is calculated as:

$$\mathrm{CVV} = N_{vessel} \times v \quad (3)$$

where N_{vessel} is the number of pixels in the segmented choroid vessels in choroid slab, v is the volume of a single pixel. Choroidal stroma volume (CSV) is defined as:

$$\mathrm{CSV} = V_{total} - CVV \quad (4)$$

Choroid vascularity index (CVI) is calculated as the vessel volume density:

$$CVI = \frac{CVV}{V_{total}} \quad (5)$$

and choroidal stroma-to-vessel ratio (CSVR) is evaluated as:

$$CSVR = \frac{CSV}{CVV} \quad (6)$$

where V_{total} is the volume of the segmented choroid slab. A larger CVI (or a smaller CSVR) indicates a denser choroidal vasculature in three-dimensions.

To study the regional distribution of choroidal thickness and vasculature measurements from a 12×12 mm scan, we created a grid composed of an 11 mm circle and a 5 mm circle centered on the fovea divided into four quadrants, but the central 2.5 mm circle was used in its entirety without quadrants.[20] Horizontal and vertical lines through the fovea were chosen because the choroidal vasculature tends to drain through vortex veins in the nasal and temporal superior and inferior quadrants, and the majority of the choroidal vessels tend to respect the horizontal meridian. This grid was applied to both the thickness maps and the segmented choroidal vasculature (Figure 2). The location of the fovea was automatically detected by searching for the local minimum thickness of retinal layers from the OCT structural scans. To study the regional distribution of choroidal thickness and vasculature measurements from a 6×6 mm scan, we used a grid that was divided into five regions. The

2.5 mm circle was used in its entirety and the 5 mm circle was divided by horizontal and vertical lines. To study the consistency of MCT & CVI measurements in the 6×6 mm and 12×12 mm scans from the same subject, we compared the regions within the 5mm circle.

Average *en face* MCT, CVV and CVI maps were generated for each age group. To do so, all *en face* MCT, CVV or CVI maps were registered at fovea and optic nerve head. The CVV and CVI distributions were calculated by applying a moving average of 600×600 μm (50×50 pixel) area. Mean maps of MCT, CVV or CVI were generated by calculating the mean values of the registered maps. The 95% normal limits for MCT, CVV or CVI maps were estimated using two standard deviations (SD) above and below the mean at each pixel and then smoothed for the final maps. Data that is either larger than three SD above mean or smaller than three SD below mean is excluded as outliers.

Normal tolerance (prediction) limits were calculated for MCT and CVI. The relationships of each of the dependent variables with age and axial length were modeled with multiple linear regression.[29] Examination of residuals demonstrated that for MCT these fits were sufficiently linear, homoscedastic, and Gaussian to calculate lower 2.5% and upper 97.5% normal tolerance (prediction) limits. Therefore we constructed normal limits by the decade of age for MCT and for each region with each scan type, adjusted to 23.5 mm of axial length. Age specific normal limits for other axial lengths can be easily obtained by adding or subtracting a constant. Normal tolerance (prediction) limits for CVI at each region of 12×12 scans were calculated using 2.5% and 97.5% percentiles.

Statistical analyses were performed using the IBM Statistical Package for the Social Sciences (SPSS), software version 21 (IBM Corporation, Armonk, New York, USA).

Results

A total of 164 normal eyes from 164 subjects ranging in age from their 20s to 80s were recruited and scanned in this study, which were also used for our previous choriocapillary study.[28] Sixteen subjects were discarded due to a failure of acquiring whole choroid layer in a 12×12 mm scan or failure to apply ‘gain control’. Four more subjects were discarded due to the poor quality of the 12×12 mm scans. A final dataset of 144 scans were used in this study. The mean age was 55 years (SD = 19) and among all the participants, 59% of them were women. The mean axial length was 23.8 mm (SD = 0.945 mm).

To validate the automated segmentation of choroids, 70 of the 144 normal subjects were randomly selected and their choroid segmentations were achieved using both the automatic method and manual segmentation. Figure 3 shows a representative comparison of choroid thickness maps (Figure 3A, B) and choroidal vasculature maps (Figure 3C, D) between manual segmentation and automatic segmentation. Qualitatively, the automatic method resulted in patterns of choroidal thickness and its vasculature that were very similar to that from manual segmentation.

Pearson’s correlation analysis and Bland-Altman agreement analysis were conducted to study the correlation and agreement of the MCT measured with automatic and manual segmentations (Figure 3E, F). From the analyses, we found that there was significant

correlation between automatic and manual segmentations in MCT measurements ($P < 0.0001$) (Figure 3E). Automatic segmentations produced smaller MCT than manual segmentations with a mean bias of -35.6 μm and a limit of agreement of -72.2 μm to 0.942 μm (Figure 3F).

Figure 4 A–D show two examples of representative choroidal thickness maps and vascular maps from eyes with a thin and a thick choroid, respectively. Pearson's correlation analysis was applied to investigate the correlation between MCT and the metrics of choroidal vessels such as CVV, CSV, CVI and CSVR (Figure 4E–H). Among all the metrics investigated, CVV and CSV showed positive correlation with MCT (all $P < 0.0001$) (Figure 4E, F), while CVI and CSVR were consistent among all subjects (61.1±1.8% and 0.64±0.05 respectively) (Figure 4G, H), indicating that the volume of choroidal vessels and choroidal stroma were larger when the choroid was thicker, however, the volume density and the volume ratio of choroidal vessels to stroma were independent of the choroid thickness.

We also studied the age-related distribution of all the metrics (Figure 5). Correlation between MCT and age is inversely significant ($r=-0.4816$, $P < 0.0001$, Pearson's correlation), which indicates that the entire choroid within the 12X12 mm scan gets thinner with the increase of age, (Figure 5A). We also observed inverse correlations of CVV and CSV metrics with age (all $P<0.0001$; Figure 5C, E), which agrees with our observations that the metrics of CVV and CSV are positively correlated with MCT. CVI and CSVR, on the other hand, remain constant and do not show correlations with age ($P=0.13$, $P=0.15$ respectively; Figure 5G). We only show the correlation graph of CVI with age because CSVR can be derived from CVI. When the subjects were grouped into different decades ranging from their 20s to 80s, we analyzed the statistical differences between decades and found that subjects in their 50s have significantly thinner choroids (smaller MCT), smaller CVV and CSV than subjects at 40s (Figure 5B, D & F), while CVI varies little across all age groups (Figure 5H).

The entire 12×12 mm scan was divided into 9 regions using a grid centered on the fovea and the regional changes in MCT and CVI for each age group were analyzed. To eliminate the influence of resolution and scale differences on the analysis, we also processed the 6×6 mm scans of the same subjects, where the scans were divided into 5 regions using a similar grid, and we compared the corresponding regions in both the 12×12 mm and 6×6 mm scans (Figure 2). Qualitatively, both choroidal thickness maps and choroidal vasculature maps derived from 12×12 mm scans and 6x6mm scans were in agreement (Figure 6). Quantitatively, Pearson's correlation analysis and Bland-Altman agreement analysis showed good correlation and agreement in MCT and CVI measurements for all 5 corresponding regions between the 12×12 mm and 6×6 mm scans (Supplemental Materials Fig. S1 & Table S1). Therefore, 12×12 mm scans are sufficient for choroid-related measurements, which is important because 12×12 mm scans provide greater choroidal FOV for clinical analyses.

Age-dependent changes were also analyzed in all sub-regions (Figure 7). Generally, the choroid was thicker in macular area and then gets thinner towards the more peripheral regions in all age groups. Overall, choroidal thickness in all regions decreased with age (Figure 7A, B). On average, the outer inferonasal region (OQ4) has thinner choroidal

measurements and the outer superotemporal region (OQ2) has thicker choroidal measurements compared with other regions of the choroid (Figure 7A). Similar trends were also observed within the regions from the 5 mm circles (Figure 7B). However, the CVI varied little among all regions and across all age groups (Figure 7C, D). MCT is larger in macular regions when compared with peripheral regions, whereas CVI does not vary much.

We calculated the normal tolerance (prediction) limits for MCT in all subregions from 12×12 mm scans (Table 1) and 6×6 mm scans (Table S2). MCT was found to be correlated with age and AL while CVI was not. Therefore, the 95% normal limits of CVI were calculated for all ages pooled (Table 2). These normal limits may be used to detect abnormalities in pathological eyes.

Average *en face* maps of the mean and 95% normal tolerance limits of MCT, CVV and CVI were generated to present the spatial distribution of choroid volume, choroidal vessel volume and regional vessel volume density in each age groups (Figure 8A–C). Overall, the choroid is thicker in macular and superior regions and thinner in inferonasal region. With the increase in age, the choroid becomes progressively thinner globally in all regions (Figure 8A). Choroidal vessel volumes follow the same pattern of choroid thickness (Figure 8B), and this is consistent with the observations that CVI varies little with ages and regions (Figure 8C).

DISCUSSION

An automated method for 3D choroidal thickness and choroidal vessel segmentation from structural SS-OCT scans was applied to a large database of normal eyes over a range of ages and good agreement was demonstrated between this automatic method and manual segmentations. We also defined several metrics for quantifying the choroid vasculature, such as CVV, CSV, CVI and CSVR. Previous studies have reported the correlation between choroidal vessels and thickness[9,20], yet the evaluations of 3D choroidal vasculature in the entire volume has not been reported. We believe our strategy of assessing the volume of choroidal vessels from the entire scan volume is the most direct and relevant approach for the study of the choroidal vasculature when compared with other measurements such as the CVI from single B-scans[9] and vessel area density from en face images[20,30]. Recent studies have used CVI measured from single B-scans obtained using EDI SD-OCT to assess vascular status of choroids in normal eyes. Subfoveal CVI has been reported in one study to range from 60.07 to 71.27% (65.61 ± 2.33%)[9], and in another study to be 49.95 ± 4.84% in normal eyes[31]. The large variation in the CVI measurements may be due to the inconsistency of the methods used and regions chosen when assessing different B-scans. By evaluating the whole choroidal vessels segmented from the entire 12×12 mm scanning region, we were able to achieve more accurate information directly from choroidal vessels over a wider FOV and to eliminate the error from subjective selections of a few B-scans, limited assessment of regions, and projection artifacts. Furthermore, the measurements on 6×6 mm scans correlate well with those from the corresponding regions on 12×12 mm scans. This indicates that our algorithm is robust among different scanning patterns with various resolutions. This is clinically useful because the volume assessment over a large field of view provides much more information about choroidal vessels than previous methods.

SS-OCT has the advantage of performing dense 12×12 mm raster scans of the macula with superior imaging of the choroid compared with SD-OCT. With the automated algorithms capable of reliably detecting the choroidal-scleral interface, it is now possible to routinely measure the choroidal thickness, CVV and CVI throughout the wide scan area.[21] Vessel segmentation can be challenging due to the lack of a "ground truth" and it depends on scan quality, therefore a relative index such as CVI may be a more clinically useful parameter than an absolute index like CVV or CSV. CSVR represents the volume ratio of the choroidal stroma and vessels and is inversely correlated with CVI. This parameter is more sensitive to the change in the choroidal stromal volume and may be as useful as CVI. CVI has shown its clinical potential in a wide range of chorioretinal diseases.[32–35] Similar to our previous study on the evaluation of age-dependent changes in choriocapillaris flow deficits,[28] we were able to generate the 95% normal limits for choroidal thickness, CVV, and CVI measurements from the entire scan area, as well as different sectors within the central and peripheral macula. We found that choroidal thickness measurements in normal subjects cover a wide range of measurements that are considered abnormal in the current literature. This wide variability in normal subjects may challenge the current concept of a pachychoroid.[36] Due to the narrow range of the CVI measurements across a normal population with highly variable choroidal thickness measurements, it may be better to classify an abnormal choroid by using just the CVI measurements alone or in conjunction with choroidal thickness measurements.

The decrease in choroidal thickness with age, which corresponds to a decrease in the choroidal vascular volume so that the CVI remains constant, suggests to us that the choroidal perfusion is likely to be responsible for the changes observed and the variability among subjects likely reflects physiological changes in normal aging that affect choroidal perfusion such as overall cardiovascular status. Using the proposed choroidal algorithms, we will be able to investigate numerous physiological parameters associated with normal aging, systemic disease, and ocular disease. In addition to the metrics investigated in this study, other metrics from structural SS-OCT scans such as choroidal vessel diameter and vessel tortuosity and complexity might be interesting to explore depending on the purpose of the studies. Unfortunately, due to the inability to detect flow throughout the larger and deeper choroidal vessels, metrics such as choroid perfusion density and choroid flow deficits are not yet possible. In addition to the correlation between choroid thickness and choroid vessels in the whole choroidal layer, it is promising to study the correlation between choroidal vessels with medium or large diameter vessels relative to the choriocapillaris. Although information of choriocapillaris cannot be achieved with this method, OCT angiography (OCTA) is well-developed to quantify choriocapillaris flow deficits and sizes.[37–39] Medium-diameter choroidal vessels in the Sattler's layer and larger-diameter choroidal vessels in the Haller's layer might also be treated separately with this method when all the choroidal vessels are segmented properly within the volumetric SS-OCT dataset. While a single 3D SS-OCT scan of 12×12 mm was used in this study, the method and assessment can be applied to different scanning protocols. It would also be promising to generate ultra-wide field-of-view choroid thickness maps and choroidal vasculature maps when coupled with montage scanning protocols.[40] We also expect that this automated 3D assessment of the choroid thickness and choroidal vasculature will provide real-time evaluations of the choroid in clinical settings.

While this method is novel with its ability to reveal choroidal morphology over a large 12×12 mm area, our method has several limitations. First of all, the segmentation of choroidal vessels and the corresponding metrics of choroidal vessels in 3D depend on the thresholding methods applied. It is difficult to find the 'ground truth' for the boundary of vessels because it relies on the contrast of image. However, in previous studies, manual segmentations have been attempted to segment choroidal vessels from single B-scans and the Otsu's method has been validated. Similar choroidal vessel density values of around 60% of the total choroid area have been reported.[9,13,14] By applying automated algorithms, this labor-consuming work can be performed automatically and quickly on thousands of B-scans, resulting in 3D information for choroidal vessels. Secondly, the applied algorithm detects the choroidal vessel bottom boundaries. It has been reported that choroid segmentation may be different depending how the posterior choroidal boundary is defined, either by the outer border of choroidal vessels, the outer border of choroidal stroma, or the inner border of the sclera.[41] Manual segmentations were published on a normal dataset following the outer border of choroidal stroma from averaged B-scans using enhanced depth imaging,[29] and the average MCT was shown to have about a 66 μm difference when compared to the segmentation following the outer border of choroidal vessels.[42] We observed a similar difference between manual and automatic segmentations. Lastly, diseased eyes, especially diseases involving thicker choroid need to be evaluated to assess the sensitivities of different metrics on different eye diseases. Previous studies have found lower CVI in eyes with diabetes mellitus[33] and diabetic retinopathy[34,43], tubercular multifocal serpiginoid choroiditis,[44] retinitis pigmentosa,[45] Stargardt disease[46]; higher CVI in eyes with central serous chorioretinopathy,[32] Vogt-Koyanagi-Harada Disease,[35] active choroidal neovascularization[47]; and no significant changes of CVI in eyes with myopic choroidal neovascularization treated with anti-VEGF[48], polypoidal choroidal vasculopathy at baseline visit compared to typical AMD[49]. It will be of interest to assess choroid vasculatures in a larger area for eyes with these diseases.

In summary, we have demonstrated that the automated assessments of choroidal thickness has shown good agreement with manual segmentations. Several metrics of choroidal vessels such as MCT, CVV, CSV, CVI and CSVR were proposed. CVV and CSV showed positive correlations with MCT in a normal database while CVI and CSVR were independent from MCT. We also showed age-related changes on the choroid-related metrics of MCT, CVV and CSV and regional distributions of choroid thickness and vasculature density measurements (MCT and CVI). The visualization of the choroid thickness and the choroidal vasculature combined with the metrics to quantitatively analyze choroidal vessels will greatly facilitate our studies into the correlations between the choroid and both ocular and systemic diseases.

Supplementary Material

Refer to Web version on PubMed Central for supplementary material.

ACKNOWLEDGEMENTS:

We thank Dr. Robert W. Knighton for suggesting and providing software for the P-spline method[50] for fitting the outer border of choroidal vessels and for useful discussions and insightful criticisms on this work.

Financial support:

Research supported by grants from the National Eye Institute (R01EY024158, R01EY028753), Carl Zeiss Meditec, the Salah Foundation, an unrestricted grant from the Research to Prevent Blindness, Inc., New York, NY, and the National Eye Institute Center Core Grant (P30EY014801) to the Department of Ophthalmology, University of Miami Miller School of Medicine. The funding organization had no role in the design or conduct of this research.

Conflict of Interest:

Here we make the following conflict of interest statements for the current study:

Dr. Gregori, Dr. Wang and Dr. Rosenfeld received research support from Carl Zeiss Meditec, Inc. Dr. Gregori and the University of Miami co-own a patent that is licensed to Carl Zeiss Meditec, Inc.

Dr. Rosenfeld is a consultant for Apellis, Boehringer-Ingelheim, Carl Zeiss Meditec, Chengdu Kanghong Biotech, Ocunexus Therapeutics, Hemera Biosciences, F. Hoffmann-La Roche Ltd., Isarna Pharmaceuticals, Ocunexus, Ocudyne, and Unity Biotechnology. Dr. Rosenfeld has equity interest in Apellis, Verana Health, and Ocudyne.

Dr. Wang discloses intellectual property owned by the Oregon Health and Science University and the University of Washington. Dr. Wang also receives research support from Tasso Inc, Moptim Inc, and Colgate Palmolive Company. He is a consultant to Insight Photonic Solutions and Carl Zeiss Meditec.

Dr. Sisternes and Dr. Durbin are employees of Carl Zeiss Meditec, Inc.

Dr. Zhou, Dr. Dai, Dr. Lyu, Dr. Noorikolouri, Dr. Zhang, Dr. Chu and Mr. Feuer have no disclosures.

REFERENCES

1. Nickla DL, Wallman J. The multifunctional choroid. Prog Retin Eye Res. 2010;29(2):144–168. [PubMed: 20044062]
2. Linsenmeier RA, Padnick-Silver L. Metabolic dependence of photoreceptors on the choroid in the normal and detached retina. Investigative Ophthalmology & Visual Science. 2000;41(10):3117–3123. [PubMed: 10967072]
3. Hayreh SS. Blood supply of the optic nerve head and its role in optic atrophy, glaucoma, and oedema of the optic disc. Br J Ophthalmol. 1969;53(11):721–748. [PubMed: 4982590]
4. Parver LM, Auker C, Carpenter DO. Choroidal Blood-Flow as a Heat Dissipating Mechanism in the Macula. Am J Ophthalmol. 1980;89(5):641–646. [PubMed: 6769334]
5. Yannuzzi LA, Rohrer KT, Tindel LJ, et al. Fluorescein angiography complication survey. Ophthalmology. 1986;93(5):611–617. [PubMed: 3523356]
6. Bloome MA. Fluorescein angiography: risks. Vision research. 1980;20(12):1083–1097. [PubMed: 7269266]
7. Mrejen S, Spaide RF. Optical coherence tomography: Imaging of the choroid and beyond. Surv Ophthalmol. 2013;58(5):387–429. [PubMed: 23916620]
8. Laviers H, Zambarakji H. Enhanced depth imaging-OCT of the choroid: a review of the current literature. Graef Arch Clin Exp. 2014;252(12):1871–1883.
9. Agrawal R, Gupta P, Tan KA, Cheung CMG, Wong TY, Cheng CY. Choroidal vascularity index as a measure of vascular status of the choroid: Measurements in healthy eyes from a population-based study. Sci Rep-Uk. 2016;6.
10. Choma MA, Sarunic MV, Yang CH, Izatt JA. Sensitivity advantage of swept source and Fourier domain optical coherence tomography. Optics Express. 2003;11(18):2183–2189. [PubMed: 19466106]
11. Yasin Alibhai A C & Witkin AJ Swept Source Optical Coherence Tomography: a Review. Current Ophthalmology Reports. 2018;6(1):7–16.
12. Lavinsky F, Lavinsky D. Novel perspectives on swept-source optical coherence tomography. Int J Retina Vitreous. 2016;2:25. [PubMed: 27847643]
13. Singh SR, Invernizzi A, Rasheed MA, et al. Wide-field Choroidal Vascularity in Healthy Eyes. Am J Ophthalmol. 2018;193:100–105. [PubMed: 29958821]

14. Ruiz-Medrano J, Ruiz-Moreno JM, Goud A, Vupparaboina KK, Jana S, Chhablani J. Age-Related Changes in Choroidal Vascular Density of Healthy Subjects Based on Image Binarization of Swept-Source Optical Coherence Tomography. Retina-J Ret Vit Dis. 2018;38(3):508–515.
15. Sonoda S, Sakamoto T, Kakiuchi N, et al. Semi-automated software to measure luminal and stromal areas of choroid in optical coherence tomographic images. Jpn J Ophthalmol. 2018;62(2):179–185. [PubMed: 29270813]
16. Sonoda S, Sakamoto T, Yamashita T, et al. Luminal and Stromal Areas of Choroid Determined by Binarization Method of Optical Coherence Tomographic Images. Am J Ophthalmol. 2015;159(6):1123–1131. [PubMed: 25790737]
17. Hirata M, Tsujikawa A, Matsumoto A, et al. Macular Choroidal Thickness and Volume in Normal Subjects Measured by Swept-Source Optical Coherence Tomography. Investigative Ophthalmology & Visual Science. 2011;52(8):4971–4978. [PubMed: 21622704]
18. Jirarattanasopa P, Ooto S, Tsujikawa A, et al. Assessment of Macular Choroidal Thickness by Optical Coherence Tomography and Angiographic Changes in Central Serous Chorioretinopathy. Ophthalmology. 2012;119(8):1666–1678. [PubMed: 22521082]
19. Wang JC, Lains I, Providencia J, et al. Diabetic Choroidopathy: Choroidal Vascular Density and Volume in Diabetic Retinopathy With Swept-Source Optical Coherence Tomography. Am J Ophthalmol. 2017;184:75–83. [PubMed: 28988899]
20. Zheng F, Gregori G, Schaal KB, et al. Choroidal thickness and choroidal vessel density in nonexudative age-related macular degeneration using swept-source optical coherence tomography imaging. Investigative ophthalmology & visual science. 2016;57(14):6256–6264. [PubMed: 27849311]
21. Zhou H, Chu Z, Zhang Q, et al. Attenuation correction assisted automatic segmentation for assessing choroidal thickness and vasculature with swept-source OCT. Biomed Opt Express. 2018;9(12):6067–6080. [PubMed: 31065413]
22. An L, Wang RKK. In vivo volumetric imaging of vascular perfusion within human retina and choroids with optical micro-angiography. Optics Express. 2008;16(15):11438–11452. [PubMed: 18648464]
23. Chen CL, Wang RK. Optical coherence tomography based angiography [Invited]. Biomed Opt Express. 2017;8(2):1056–1082. [PubMed: 28271003]
24. Kashani AH, Chen CL, Gahm JK, et al. Optical coherence tomography angiography: A comprehensive review of current methods and clinical applications. Prog Retin Eye Res. 2017;60:66–100. [PubMed: 28760677]
25. Kirby MA, Li C, Choi WJ, Gregori G, Rosenfeld P, Wang R. Why choroid vessels appear dark in clinical OCT images. Paper presented at: Ophthalmic Technologies XXVIII2018.
26. Wang RKK, Kirby M, Li CX, Choi WJ, Gregori G, Rosenfeld PJ. An explanation for why choroidal blood vessels appear dark on clinical OCT images. Investigative Ophthalmology & Visual Science. 2017;58(8):4754–4754. [PubMed: 28973319]
27. Claudon M, Tranquart F, Evans DH, Lefevre F, Correas JM. Advances in ultrasound. Eur Radiol. 2002;12(1):7–18. [PubMed: 11868070]
28. Zheng F, Zhang QQ, Shi YY, et al. Age-dependent Changes in the Macular Choriocapillaris of Normal Eyes Imaged With Swept-Source Optical Coherence Tomography Angiography. Am J Ophthalmol. 2019;200:110–122. [PubMed: 30639367]
29. Abbey AM, Kuriyan AE, Modi YS, et al. Optical Coherence Tomography Measurements of Choroidal Thickness in Healthy Eyes: Correlation With Age and Axial Length. Osli Retina. 2015;46(1):18–24. [PubMed: 25559504]
30. Ogawa Y, Maruko I, Koizumi H, Iida T. Quantification of Choroidal Vasculature by High-Quality Structure En Face Swept-Source Optical Coherence Tomography Images in Eyes with Central Serous Chorioretinopathy. Retina. 2018.
31. Agrawal R, Wei X, Goud A, Vupparaboina KK, Jana S, Chhablani J. Influence of scanning area on choroidal vascularity index measurement using optical coherence tomography. Acta Ophthalmol. 2017;95(8):e770–e775. [PubMed: 28470942]

32. Ambiya V, Goud A, Rasheed MA, Gangakhedkar S, Vupparaboina KK, Chhablani J. Retinal and choroidal changes in steroid-associated central serous chorioretinopathy. Int J Retina Vitreous. 2018;4:11. [PubMed: 29619248]
33. Tan KA, Laude A, Yip V, Loo E, Wong EP, Agrawal R. Choroidal vascularity index - a novel optical coherence tomography parameter for disease monitoring in diabetes mellitus? Acta Ophthalmol. 2016;94(7):E612–E616. [PubMed: 27151819]
34. Kim M, Ha MJ, Choi SY, Park YH. Choroidal vascularity index in type-2 diabetes analyzed by swept-source optical coherence tomography. Sci Rep-Uk. 2018;8.
35. Agrawal R, Li LKH, Nakhate V, Khandelwal N, Mahendradas P. Choroidal Vascularity Index in Vogt-Koyanagi-Harada Disease: An EDI-OCT Derived Tool for Monitoring Disease Progression. Transl Vis Sci Techn. 2016;5(4).
36. Gallego-Pinazo R, Dolz-Marco R, Gomez-Ulla F, Mrejen S, Freund KB. Pachychoroid diseases of the macula. Med Hypothesis Discov Innov Ophthalmol. 2014;3(4):111–115. [PubMed: 25756060]
37. Zhang QQ, Shi YY, Zhou H, et al. Accurate estimation of choriocapillaris flow deficits beyond normal intercapillary spacing with swept source OCT angiography. Quant Imag Med Surg. 2018;8(7):658–666.
38. Zhang QQ, Zheng F, Motulsky EH, et al. A Novel Strategy for Quantifying Choriocapillaris Flow Voids Using Swept-Source OCT Angiography. Investigative Ophthalmology & Visual Science. 2018;59(1):203–211. [PubMed: 29340648]
39. Chu ZD, Zhou H, Cheng YX, Zhang QQ, Wang RK. Improving visualization and quantitative assessment of choriocapillaris with swept source OCTA through registration and averaging applicable to clinical systems. Sci Rep-Uk. 2018;8.
40. Zhang QQ, Lee CS, Chao J, et al. Wide-field optical coherence tomography based microangiography for retinal imaging. Sci Rep-Uk. 2016;6:22017.
41. Huynh E, Chandrasekera E, Bukowska D, McLenachan S, Mackey DA, Chen FK. Past, Present, and Future Concepts of the Choroidal Scleral Interface Morphology on Optical Coherence Tomography. Asia Pac J Ophthalmol (Phila). 2017;6(1):94–103. [PubMed: 28161920]
42. Vuong VS, Moisseiev E, Cunefare D, Farsiu S, Moshiri A, Yiu G. Repeatability of Choroidal Thickness Measurements on Enhanced Depth Imaging Optical Coherence Tomography Using Different Posterior Boundaries. Am J Ophthalmol. 2016;169:104–112. [PubMed: 27345731]
43. Kim M, Kim RY, Kim JY, Park YH. Correlation of systemic arterial stiffness with changes in retinal and choroidal microvasculature in type 2 diabetes. Sci Rep-Uk. 2019;9.
44. Agarwal A, Agrawal R, Khandelwal N, et al. Choroidal Structural Changes in Tubercular Multifocal Serpiginoid Choroiditis. Ocul Immunol Inflamm. 2018;26(6):838–844. [PubMed: 29020533]
45. Tan R, Agrawal R, Taduru S, Gupta A, Vupparaboina K, Chhablani J. Choroidal Vascularity Index in Retinitis Pigmentosa: An OCT Study. Osli Retina. 2018;49(3):191–197. [PubMed: 29554387]
46. Ratra D, Tan R, Jaishankar D, et al. Choroidal Structural Changes and Vascularity Index in Stargardt Disease on Swept Source Optical Coherence Tomography. Retina-J Ret Vit Dis. 2018;38(12):2395–2400.
47. Invernizzi A, Benatti E, Cozzi M, et al. Choroidal Structural Changes Correlate With Neovascular Activity in Neovascular Age Related Macular Degeneration. Investigative Ophthalmology & Visual Science. 2018;59(10):3836–3841. [PubMed: 30073357]
48. Ng WY, Ting DSW, Agrawal R, et al. Choroidal Structural Changes in Myopic Choroidal Neovascularization After Treatment With Antivascular Endothelial Growth Factor Over 1 Year. Investigative Ophthalmology & Visual Science. 2016;57(11):4933–4939. [PubMed: 27654420]
49. Ting DSW, Yanagi Y, Agrawal R, et al. Choroidal Remodeling in Age-related Macular Degeneration and Polypoidal Choroidal Vasculopathy: A 12-month Prospective Study. Sci Rep-Uk. 2017;7.
50. Knighton RW, Gregori G. The Shape of the Ganglion Cell plus Inner Plexiform Layers of the Normal Human Macula. Investigative Ophthalmology & Visual Science. 2012;53(11):7412–7420. [PubMed: 23033389]

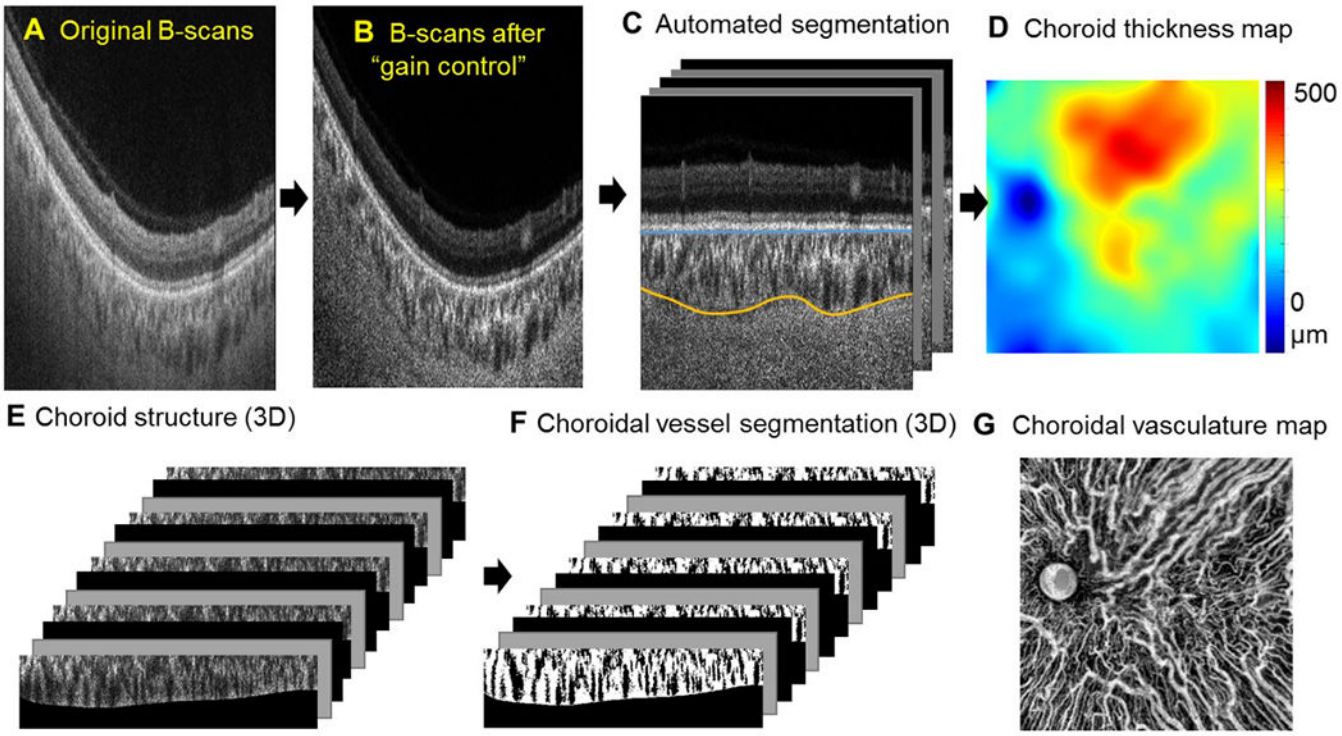

Figure 1.

Flow chart for automatic assessment of choroid thickness and the choroidal vasculature. Signals in the regular OCT B-scans (A) were converted to enhanced signals with attenuation correction (B). (C) Automatic segmentation of choroid slab. The Bruch's membrane (blue line) and outer boundaries of the choroidal vessels (yellow line) were detected through graph search methods. (D) *En face* choroidal thickness map. (E, F) Choroidal vessels were segmented in the whole volume and were presented as an *en face* choroidal vasculature map (G).

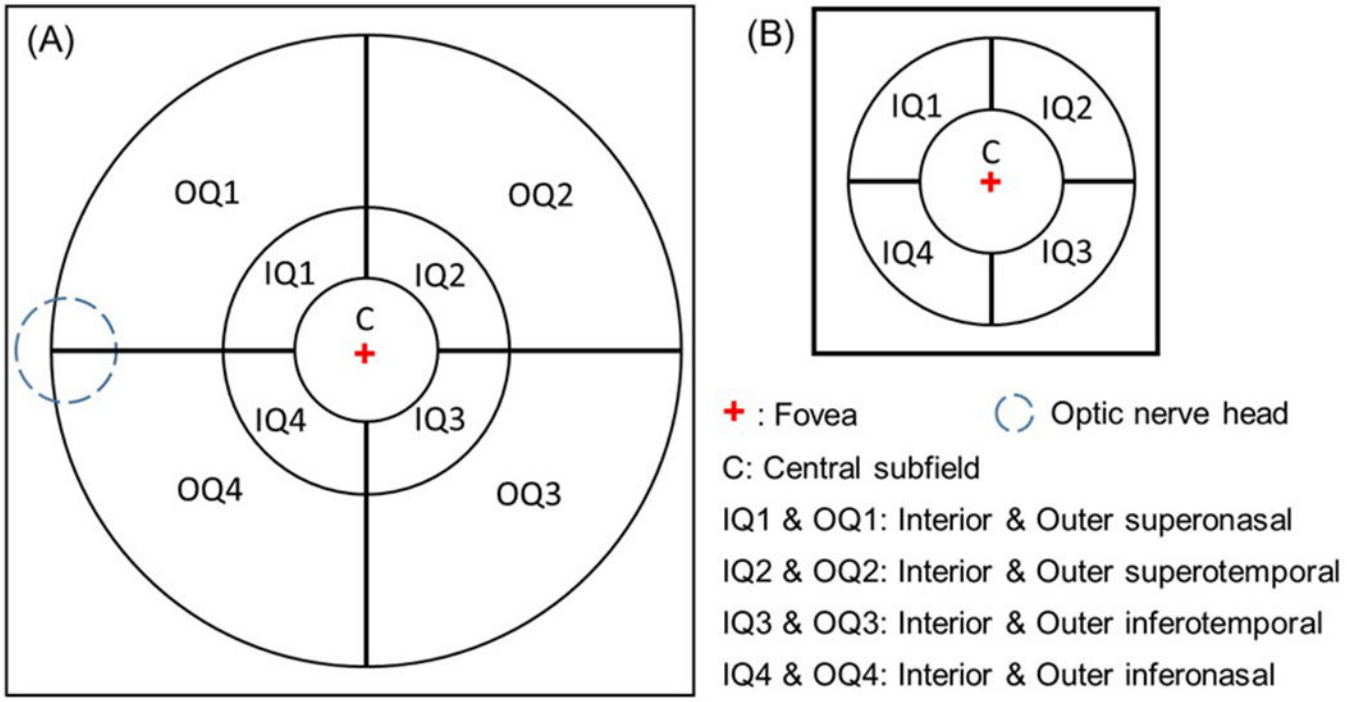

Figure 2.

Regional analysis of choroidal thickness and vessel volume using a grid centered on the fovea. (A) The grid used for the 12×12 mm scans was divided into 9 regions using 2.5 mm, 5 mm, 11 mm circles with horizontal and vertical lines added outside the 2.5 mm circle to divide the 5 mm and 11mm circles into quadrants. (B) The grid used for the 6×6 mm scans was divided into 5 regions using 2.5 mm and 5 mm circles with horizontal and vertical lines added outside the 2.5 mm circle to divide the 5 mm circle into quadrants.

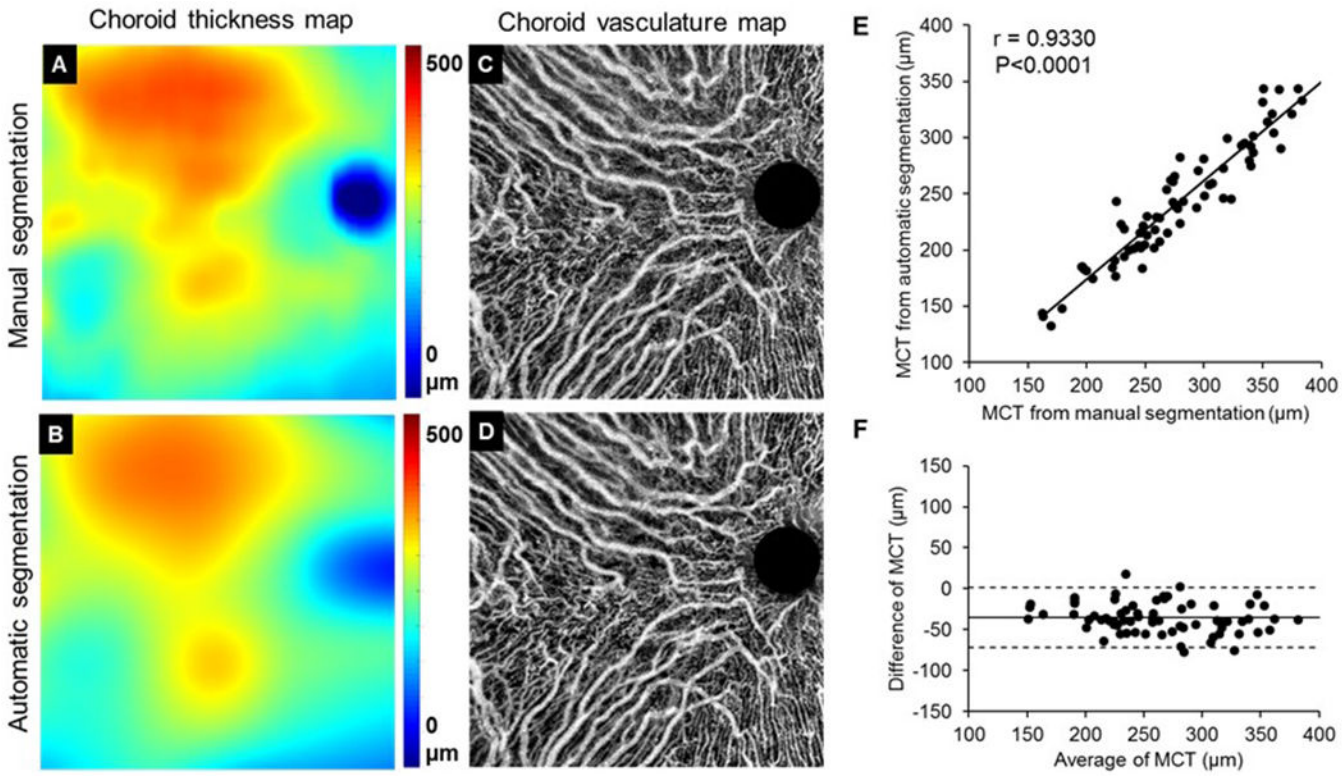

Figure 3.

Validation of automated choroid segmentations with manual segmentations. (A, B) Choroid thickness map from manual segmentation (A) and automatic segmentation (B), respectively. (C, D) Choroidal vasculature maps from manual segmentation (C) and automatic segmentation (D), respectively. (E, F) Pearson's correlation analysis and Bland-Altman agreement analysis on MCT between automatic and manual segmentations. MCT: mean choroidal thickness.

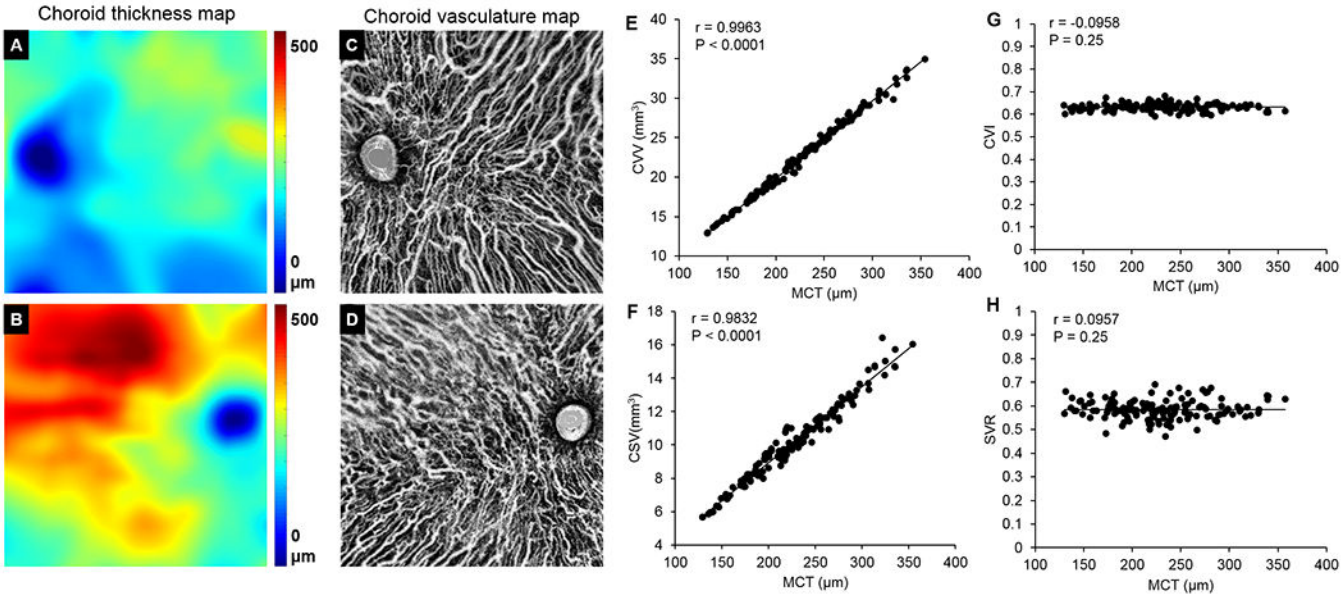

Figure 4.

Correlation study between choroidal vasculature and choroid thickness. (A-D) Representative choroid thickness map (A&B) and choroidal vasculature map (C&D) for thin and thick choroids respectively. (E-H) Correlation between MCT and the metrics of choroidal vasculatures (CVV, CSV, CVI and SVR). Data was analyzed through Pearson's correlation analysis. MCT: mean choroidal thickness. CVV: choroidal vessel volume. CSV: choroidal stroma volume. CVI: choroid vascularity index. SVR: stroma to vessel ratio.

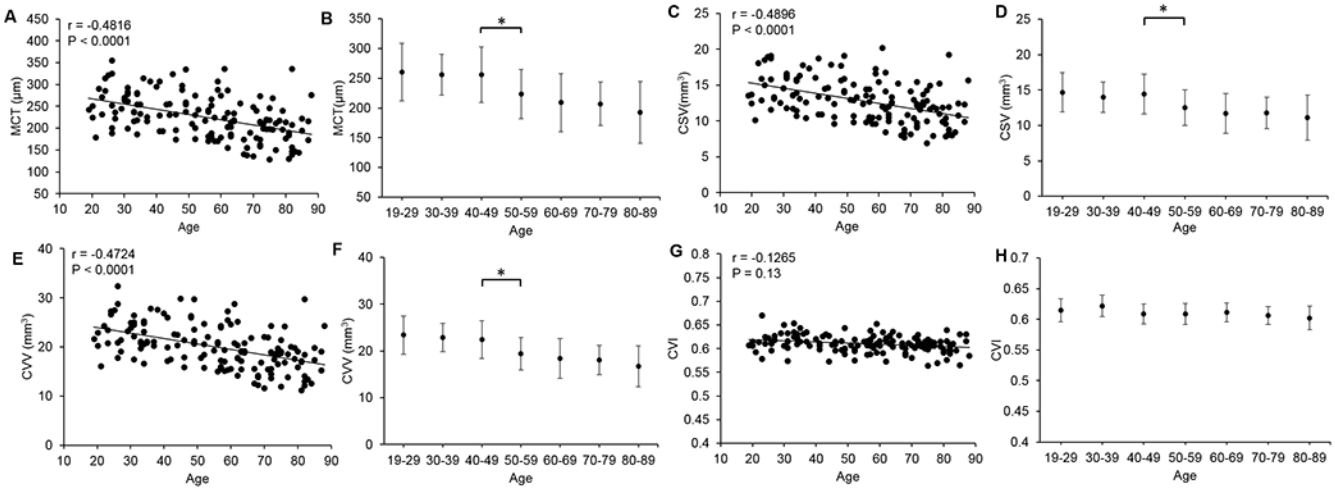

Figure 5.

Age-related distribution of mean choroidal thickness (MCT), choroidal vessel volume (CVV), choroidal stromal volume (CSV), and choroid vascularity index (CVI). (A, C, E, G) Correlation between age and choroidal metrics was analyzed through Pearson's correlation analysis. (B, D, F, H) Distribution of choroid metrics with a series of age groups. (*, P<0.05, two-tailed t-test).

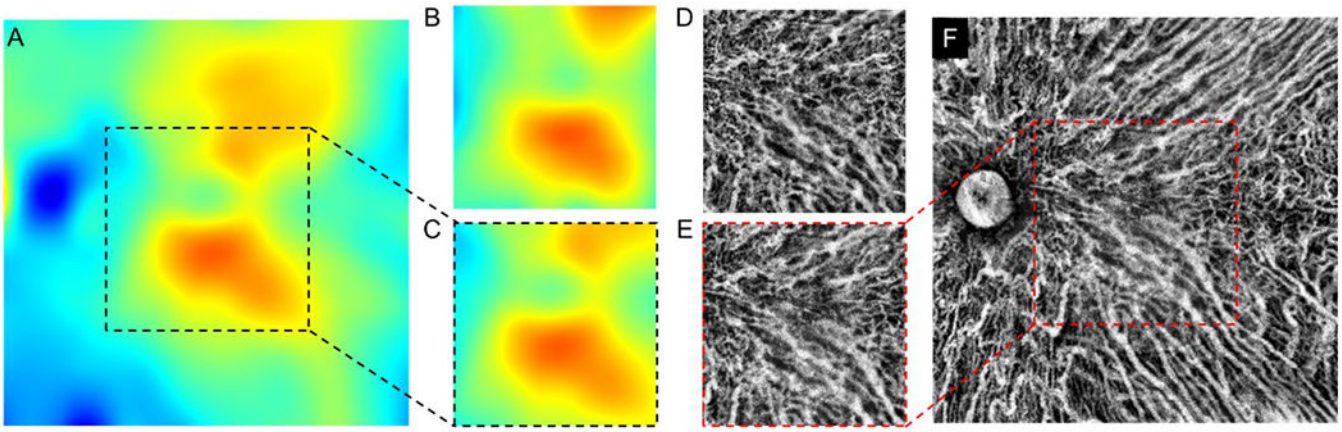

Figure 6.

Choroidal thickness map and choroidal vasculature map of 12×12 mm (A, F) and 6×6 mm (B, D) scans from the same subject. For comparison with the 6×6 mm scans, the 6×6 mm regions from the 12×12mm scans were cropped to show the choroidal thickness map (C) and the choroidal vasculature map (D).

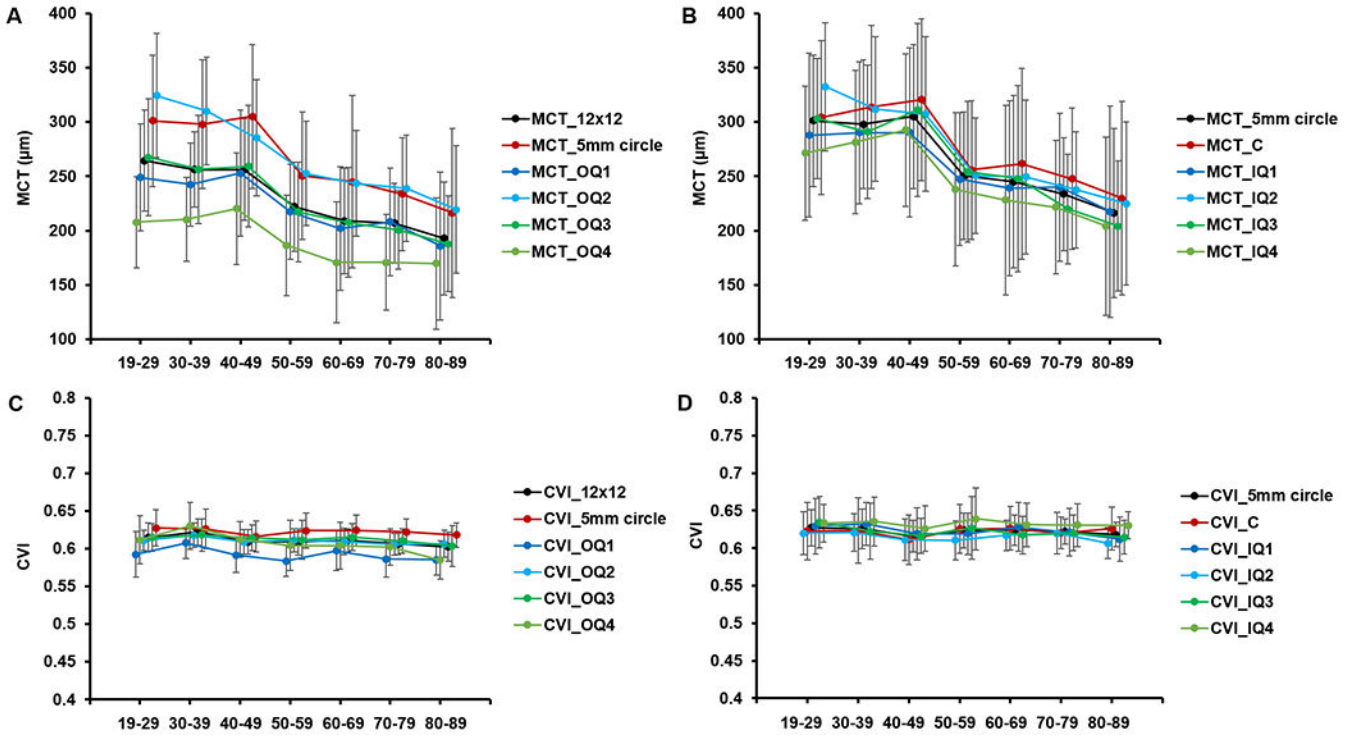

Figure 7.

Regional change of mean choroid thickness (MCT) and choroid vascularity index (CVI) with aging. Data is represented as mean ± SD. (A) Age-dependent regional changes in MCT at outer quadrant regions, entire 12x12 mm and entire 5mm circle; (B) Age-dependent regional changes in MCT at inner quadrant regions, entire 5mm circle and central 2.5mm circle; (C) Age-dependent regional changes in CVI at outer quadrant regions, entire 12x12 mm and entire 5mm circle; and (D) Age-dependent regional change in CVI at inner quadrant regions, entire 5mm circle and central 2.5mm circle. Please refer to Figure 2 for abbreviations of regions.

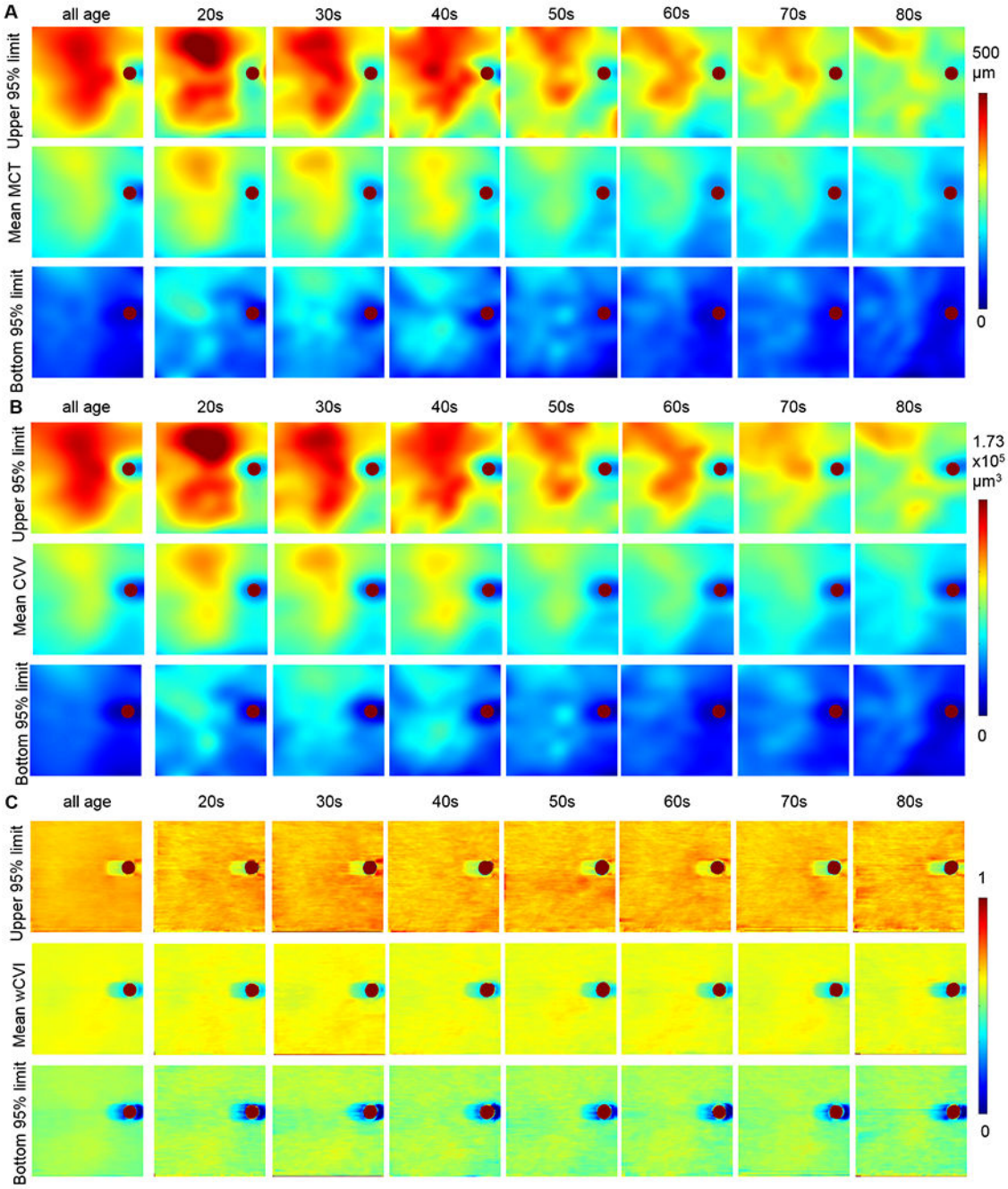

Figure 8.

Mean and 95% normal tolerance limit en face 12×12 mm maps of choroid thickness (MCT) (A), choroid vessel volume (CVV) (B) and choroid vascularity index (CVI) (C) in all ages and in each age decades.

Table 1.

95% normal tolerance limit of mean choroidal thickness (MCT) by age and region from 12×12 mm scans. Axial length (AL) = 23.5mm*.

95% Normal Range of Choroid Mean Thickness by Each Decade of Age (μm, AL=23.5mm)							
Regions Quantified	**Age Group**						
	19-29	**30-39**	**40-49**	**50-59**	**60-69**	**70-79**	**80-89**
C (2.5-mm circle)	179.1 - 481.8	163.0 - 464.2	146.6 - 446.8	130.0 - 429.8	113.0 - 413.0	95.8 - 396.6	78.2 - 380.4
5-mm circle	190.4 - 449.8	173.5 - 431.5	156.3 - 413.6	138.9 - 395.8	121.3 - 378.3	103.3 - 361.1	85.2 - 344.1
11-mm circle	189.7 - 383.2	174.7 - 367.2	159.6 - 351.5	144.3 - 336.0	128.9 - 320.6	113.2 - 305.5	97.4 - 290.5
IQ1	157.8 - 456.8	143.7 - 441.2	129.4 - 425.9	114.7 - 410.8	99.7 - 396.1	84.5 - 381.6	68.9 - 367.4
IQ2	205.6 - 465.0	186.1 - 444.1	166.3 - 423.6	146.3 - 403.2	126.1 - 383.1	105.5 - 363.3	84.8 - 343.7
IQ3	186.6 - 456.2	168.1 - 436.4	149.3 - 416.8	130.3 - 397.4	111.1 - 378.3	91.5 - 359.5	71.8 - 340.9
IQ4	158.5 - 443.4	143.2 - 426.6	127.6 - 410.1	111.7 - 393.9	95.6 - 378.0	79.2 - 362.3	62.5 - 346.9
OQ1	155.5 - 366.1	144.0 - 353.6	132.4 - 341.2	120.5 - 329.1	108.5 - 317.2	96.2 - 305.4	83.7 - 293.9
OQ2	219.1 - 429.2	201.1 - 410.1	182.9 - 391.2	164.5 - 372.5	145.8 - 354.0	127.0 - 335.8	108.0 - 317.7
OQ3	175.4 - 371.4	161.1 - 356.1	146.6 - 340.9	131.9 - 326.0	117.0 - 311.2	102.0 - 296.7	86.7 - 282.3
OQ4	127.4 - 321.3	117.6 - 310.5	107.6 - 299.9	97.4 - 289.4	87.0 - 279.2	76.5 - 269.1	65.7 - 259.2
12x12 mm	185.9 - 360.3	172.4 - 346.0	158.8 - 331.8	145.1 - 317.8	131.2 - 304.0	117.1 - 290.4	102.8 - 276.9

*The MCT were corrected by axial length (AL) as: $MCT_{corr} = MCT - \alpha \times AL$, where α is 24.9 μm/mm.

Table 2.

95% normal tolerance limit of choroidal vessel volume density (CVVD) by region from 12×12 mm scans.

95% Normal Range of Choroidal Vessel Volume Density (all ages)	
Regions Quantified	**Normal Range**
C (2.5-mm circle)	0.55 - 0.68
5-mm circle	0.58 - 0.67
11-mm circle	0.57 - 0.65
IQ1	0.56 - 0.69
IQ2	0.56 - 0.67
IQ3	0.56 - 0.68
IQ4	0.57 - 0.69
OQ1	0.54 - 0.65
OQ2	0.58 - 0.64
OQ3	0.57 - 0.65
OQ4	0.54 - 0.68
12x12 mm	0.57 - 0.65